Supporting Information

Highly active and durable non-precious-metal catalyst encapsulated in carbon nanotubes for hydrogen evolution reaction

Jiao Deng,[§] Pengju Ren,[§] Dehui Deng,* Liang Yu, Fan Yang, Xinhe Bao*

State Key Laboratory of Catalysis, Dalian Institute of Chemical Physics, Chinese Academy of Sciences, Zhongshan Road 457, Dalian 116023, China.

[§]These authors have contributed equally.

*E-mail: dhdeng@dicp.ac.cn; xhbao@dicp.ac.cn; Fax: +86-411-84379128; Tel: +86-411-84686637.

Experimental Section

Materials preparation.

All the chemicals were of analytical grade and used as received without further purification. The N-doped CNTs encapsulated metal, Fe@NCNTs, Co@NCNTs and FeCo@NCNTs were prepared through a chemical vapor deposition (CVD) method. In a typical approach, metal catalysts (Fe, Co or FeCo) were first supported onto MgO through a impregnation method by using the precursors of $Fe(NO_3)_3$ and $Co(NO_3)_2$, with a loading of 2 wt.% Fe, 2 wt.% Co and 1 wt.% Fe + 1 wt.% Co, respectively. Then, the catalysts were transferred into a CVD furnace, temperature programmed from room temperature to 700 ^oC under 20% H_2/Ar, followed by bubbling pyridine with 80 mL min^{-1} Ar for 20 minutes. Finally, the resulting samples were treated in 0.5 M H_2SO_4 aqueous solution at 90 ^oC for 4 h, followed by washing in distilled water and drying at 100 ^oC for 12 h. Fe@NCNTs-NH, Co@NCNTs-NH and FeCo@NCNTs-NH were prepared by using a same CVD process with the aid of an additional 30 mL min^{-1} NH_3 during bubbling pyridine. The MWCNTs and SWCNTs were purchased from Chengdu Organic Chemicals Co. Ltd. CAS, which were further treated by refluxing in concentrated HNO_3 under 130 ^oC for 12 h and 2 h, respectively, according to our previous study.[1] The MWCNTs-NH was obtained via treating the MWCNTs in NH_3 under 700 ^oC for 20 min.

Materials characterization.

Scanning electron microscopy (SEM) and scanning transmission electron microscopy (STEM) were conducted on Hitachi S5500 operated at 30 kV. Transmission electron microscopy (TEM) was carried out on a FEI Tecnai F30 microscope and a G^2 microscope operated at an accelerating voltage of 300 and 120 kV, respectively. Elemental mapping by energy dispersive X-ray spectroscopy (EDX) was carried out on a FEI Tecnai F30 microscope operated at an accelerating voltage of 300 KV. X-ray diffraction (XRD) measurements were conducted on a Rigaku D/MAX 2500 diffractometer with Cu Kα radiation (λ=1.5418 Å) at 40 kV and 200 mA. X-ray photoelectron spectroscopy (XPS) measurements were carried out on a VG ESCALAB MK2 spectroscope used Al Kα X-rays as the excitation source with a voltage of 12.5 kV and power of 250 W. Inductively coupled plasma atomic emission spectroscopy (ICP-AES) was carried out in SHIMADZU ICPS-8100 and the samples for ICP-AES analysis were first heated at 800 ^oC for 5 h in air, followed by treatment in aqua regia.

Electrochemical analysis.

HER polarization curve tests were conducted on a 2273 potentiostat/galvanostat with a three-electrode electrochemical cell equipped with a gas flow controlling system. Graphite rod was used as the counter electrode and Ag/AgCl (saturated KCl-filled) as the reference electrode. A glassy carbon rotating disk electrode with a diameter of 5 mm covered by a thin catalyst film was used as the working electrode. Typically, 5 mg catalyst was suspended in 2 mL ethanol with 50 μL Nafion solution (5 wt.%, Du Pont) to form homogeneous ink assisted by ultrasound. Then 25 μL of the ink was spread onto the surface of glassy carbon by a micropipette and dried under room temperature. The final loading for all catalysts and 40% commercial Pt/C electrocatalys on work electrode is 0.32 mg/cm^2. Experiments were conducted in an N_2 saturated 0.1 M H_2SO_4 electrolyte at 25 ^oC. The potential range was from 0 to -1.0 V (vs. Ag/AgCl) and the scan rate was 2 mV s^{-1}. Before measurements, the samples were repeatedly swept from -0.3 to +0.7 V (vs. Ag/AgCl) in an N_2-protected 0.1 M H_2SO_4 electrolyte until a steady voltammogram curve had been obtained.

The reversible hydrogen electrode (RHE) calibration was performed in H_2-

saturated 0.1 M H_2SO_4 with a Pt wire as the work electrode. The potential was swept near the thermodynamic potential for H^+/H_2 reaction and when the current crossed zero, the potential at there was adopted to be the potential for H^+/H_2 reaction.

Electrolyte	**Reference electrode**	**Thermodynamic potential for hydrogen electrode**	**Conversion equation**
0.1 M H_2SO_4	Ag/AgCl	-0.268 V vs. Ag/AgCl	E(RHE) = E(Ag/AgCl) + 0.268 V

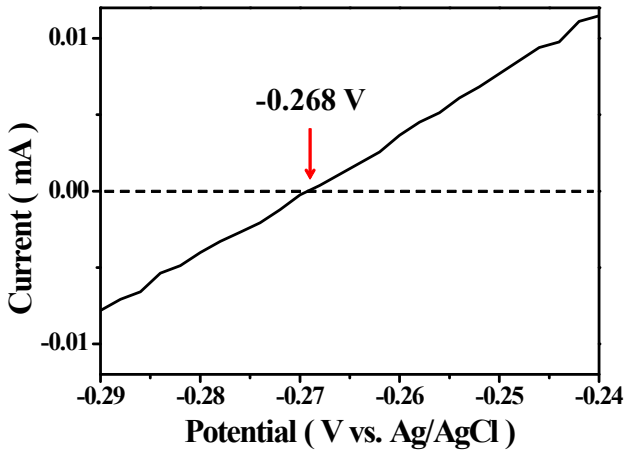

All these materials synthesis and the HER performance mentioned above were well reproducible in our laboratory.

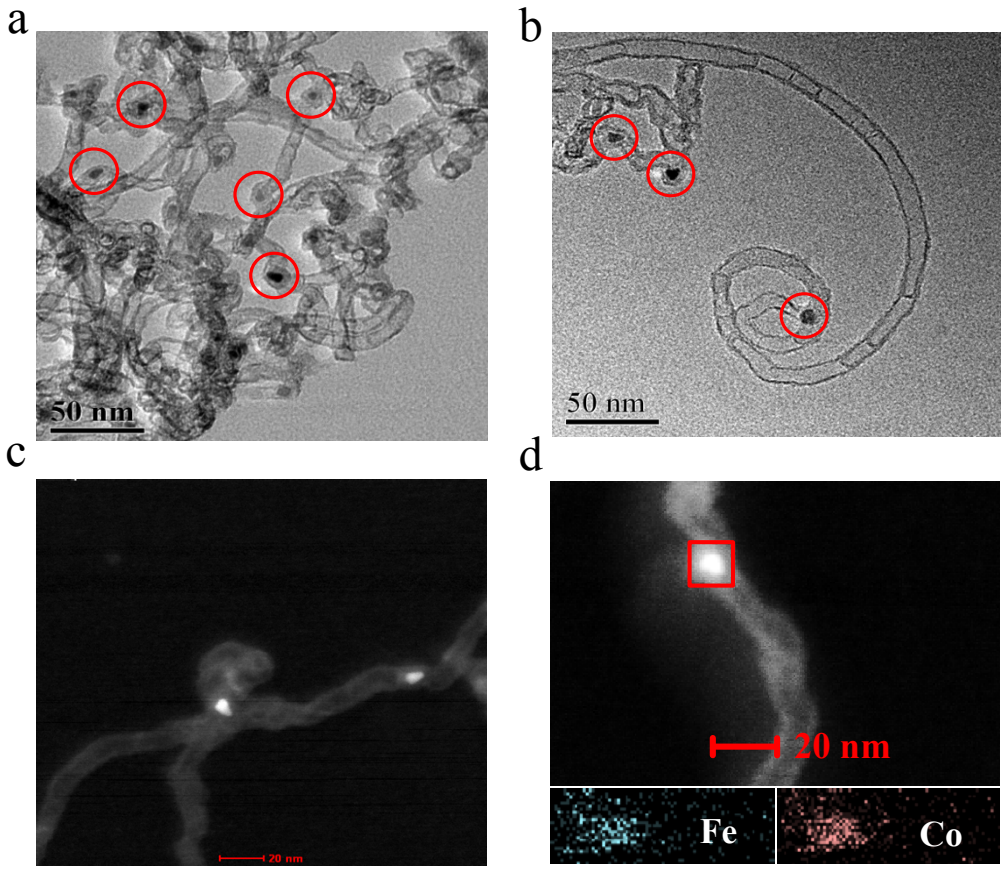

Figure S1. (a), (b) TEM images of FeCo@NCNTs with the red circles showing the encapsulated metal NPs. (c) High-angle annular-dark field (HAADF) image of FeCo@NCNTs. (d) Elemental mapping of Fe and Co for one metal NP of FeCo@NCNTs in the area marked by a red square.

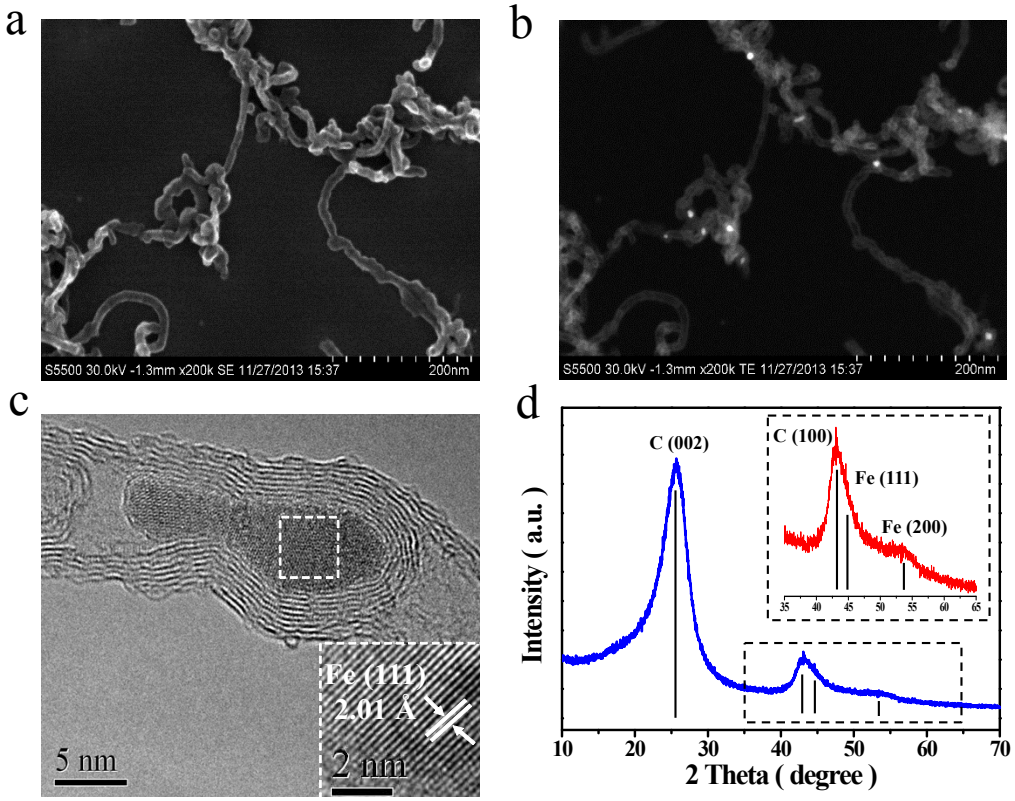

Figure S2. (a) SEM image of Fe@NCNTs. (b) STEM image of Fe@NCNTs at the same region with the SEM. (c) HRTEM image of Fe@NCNTs with the inset showing the (111) crystal plane of the Fe nanoparticle. (d) XRD pattern of Fe@NCNTs with the inset showing the partial enlarged detail between the 35 degree and 65 degree.

SEM image (Figure S2a) and the corresponding STEM image (Figure S2b) showed the tubular morphology of Fe@NCNTs and the encapsulated metal NPs as the bright dots in figure S2b. HRTEM image (Figure S2c) exhibited that the metal NP was completely coated by the graphitic carbon shells and the NP exhibits a *d* spacing of 2.01 Å, corresponding to the (111) plane of metallic Fe. XRD pattern (Figure S2d) also showed the (111) and (200) lattice planes of metallic Fe. These results indicate that the metallic Fe NPs were completely encapsulated inside the CNTs.

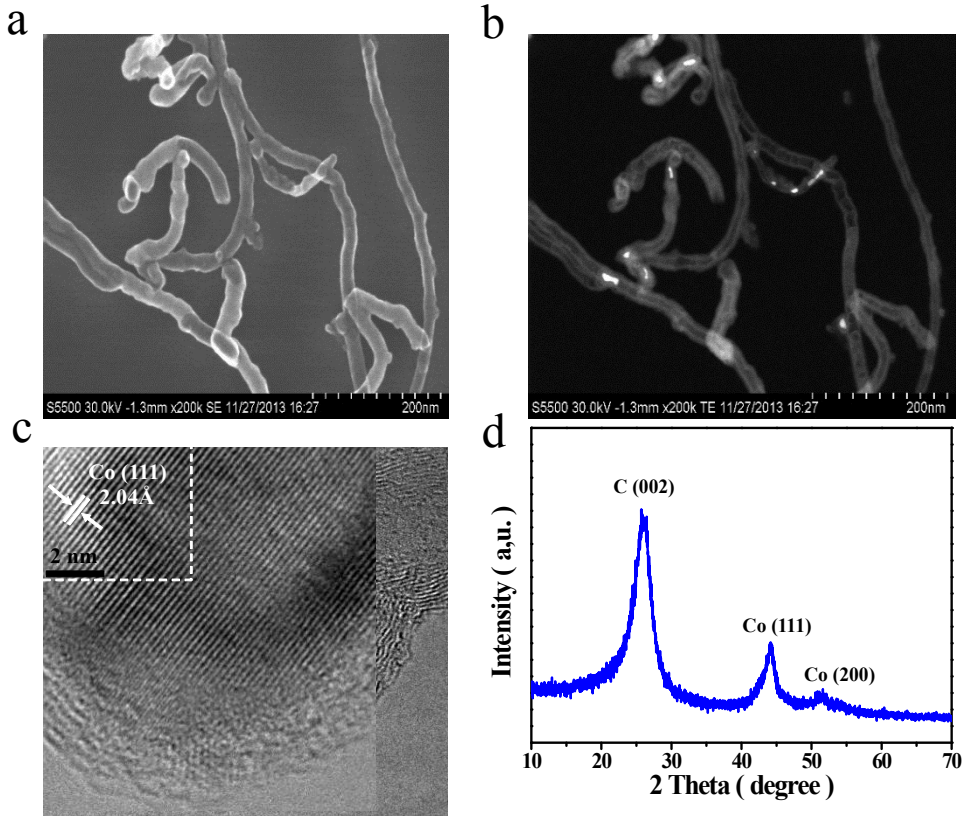

Figure S3. (a) SEM image of Co@NCNTs. (b) STEM image of Co@NCNTs at the same region with the SEM. (c) HRTEM image of Co@NCNTs with the inset showing the (111) crystal plane of the Co nanoparticle. (d) XRD pattern of Co@NCNTs.

SEM image (Figure S3a) and the corresponding STEM image (Figure S3b) showed the tubular morphology of Co@NCNTs and the encapsulated metal NPs as the bright dots in the figure S3b. HRTEM image (Figure S3c) exhibited that the metal NP was completely coated by the graphitic carbon shells and the NP exhibits a *d* spacing of 2.04 Å, corresponding to the (111) plane of metallic Co. XRD pattern (Figure S3d) also showed the (111) and (200) lattice planes of metallic Co. These results indicate that the metallic Co NPs were completely encapsulated inside the CNTs.

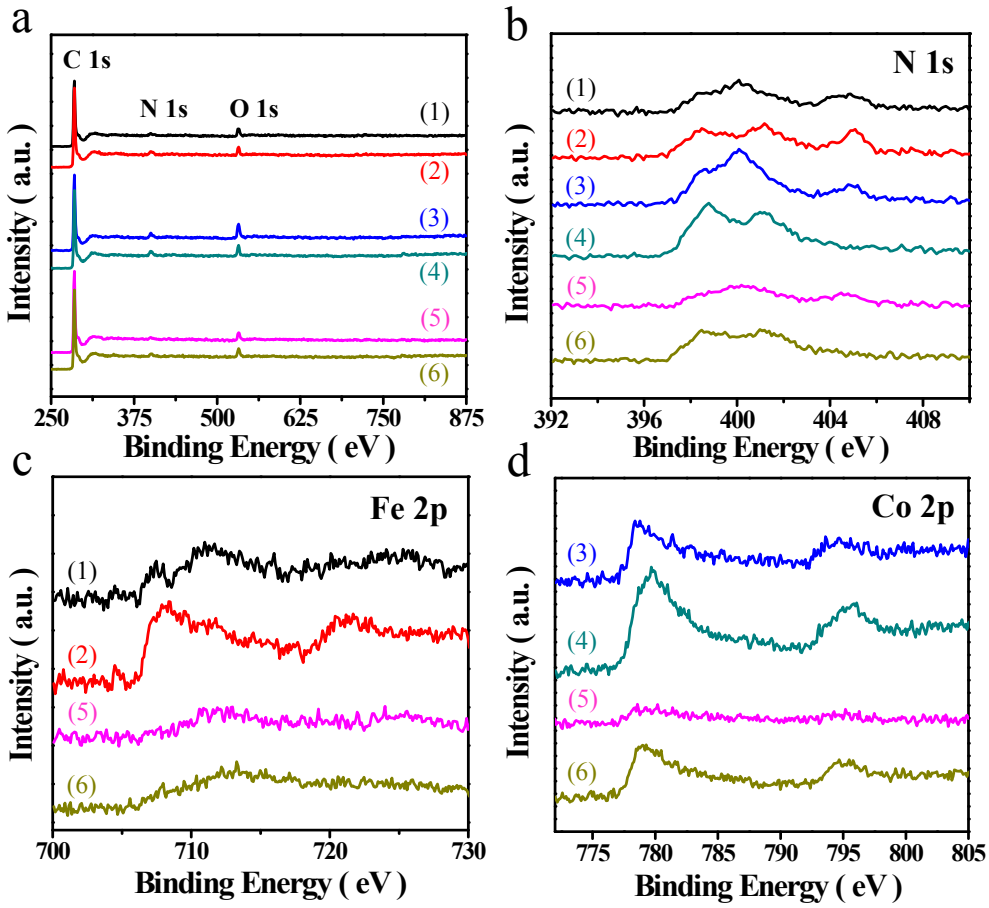

Figure S4. XPS spectra: (a) wide spectrum; (b) N 1s spectrum; (c) Fe 2p spectrum; (d) Co 2p spectrum. The numbers (1), (2), (3), (4), (5) and (6) represent Fe@NCNTs, Fe@NCNTs-NH, Co@NCNTs, Co@NCNTs-NH, FeCo@NCNTs and FeCo@NCNTs-NH, respectively.

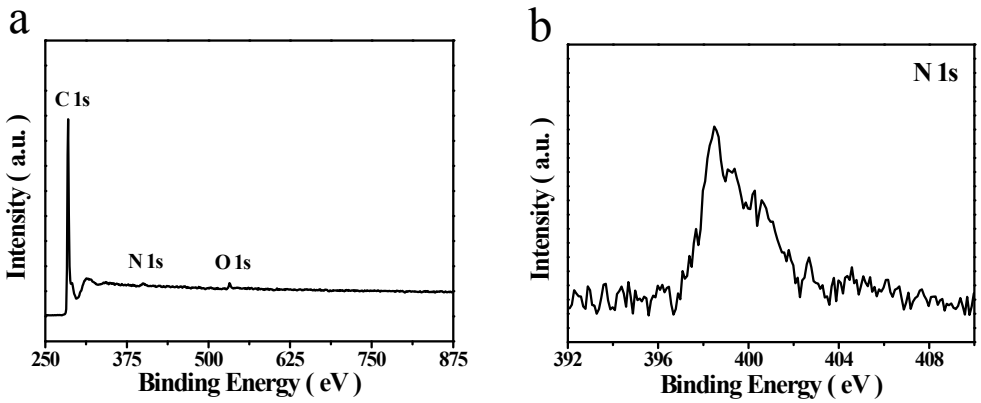

Figure S5. XPS spectra of MWCNTs-NH: (a) wide spectrum; (b) N 1s spectrum. The N content in MWCNTs-NH estimated is about 1.3 wt. %.

Table S1. Chemical compositions of Fe@NCNTs, Fe@NCNTs-NH, Co@NCNTs, Co@NCNTs-NH, FeCo@NCNTs and FeCo@NCNTs-NH estimated from XPS and ICP measurements.

Sample	C (wt. %)	O (wt. %)	N (wt. %)	Fe (wt. %)	Co (wt. %)
Fe@NCNTs	87.9	6.6	3.6	1.9	–
Fe@NCNTs-NH	88.3	4.8	4.1	2.8	–
Co@NCNTs	83.2	8.9	4.8	–	3.1
Co@NCNTs-NH	85.1	6.8	5.2	–	2.9
FeCo@NCNTs	89.9	5.9	2.7	0.8	0.7
FeCo@NCNTs-NH	87.6	5.6	3.8	1.2	1.8

C, O and N contents were detected by XPS, Fe and Co contents were detected by ICP.

Table S2. Summary of representative non-precious-metal HER catalysts.

Catalyst	Catalyst amount (mg/cm^2)	Electrolyte solution	Onset overpotential (vs. RHE)	Reference
FeCo@NCNTs-NH	0.32	0.1 M H_2SO_4	~70 mV	This work
FeCo@NCNTs	0.32	0.1 M H_2SO_4	~110 mV	This work
MoS_2/RGO	0.28	0.5 M H_2SO_4	~100 mV	[2]
$NiMoN_x$/C	0.25	0.1 M $HClO_4$	78 mV	[3]
MoN/C	0.25	0.1 M $HClO_4$	157 mV	[3]
MoB	2.5	1 M H_2SO_4	~100 mV	[4]
Mo_2C	1.4	1 M H_2SO_4	~100 mV	[4]
Cu_2MoS_4	0.041	0.5 M H_2SO_4	135 mV	[5]
Fe-WCN	0.4	0.05 M H_2SO_4	~100 mV	[6]
Mo_2C/CNT	2	0.1 M $HClO_4$	63 mV *	[7]

* The overpotential shown here is at 1 mA/cm^2 due to the reference did not provide the onset overpotential.

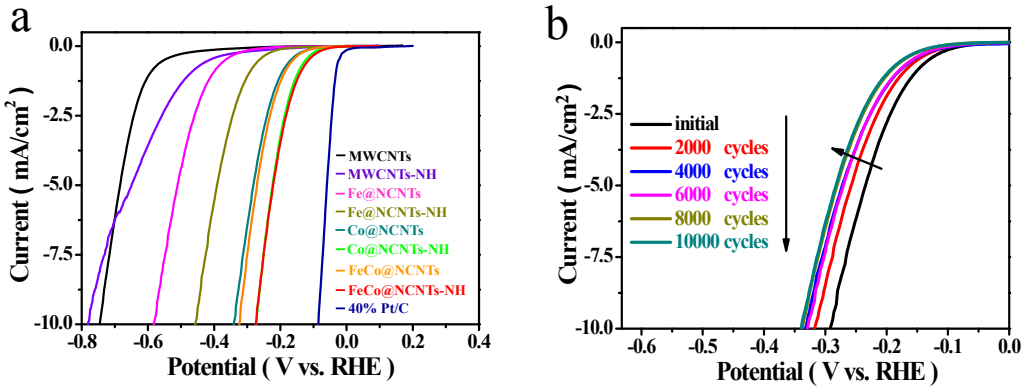

Figure S6. (a) Polarization curves of MWCNTs-NH, Fe@NCNTs-NH, Co@NCNTs-NH, FeCo@NCNTs-NH in comparison with the corresponding MWCNTs, Fe@NCNTs, Co@NCNTs and FeCo@NCNTs, respectively. (b) Durability measurement of FeCo@NCNTs-NH: polarization curves recorded initially and after every 2000 CV sweeps between +0.77 and -0.13 V (vs. RHE) at 100 mV s^{-1}. All the polarization curves were performed in 0.1 M H_2SO_4 at a scan rate of 2 mV s^{-1}.

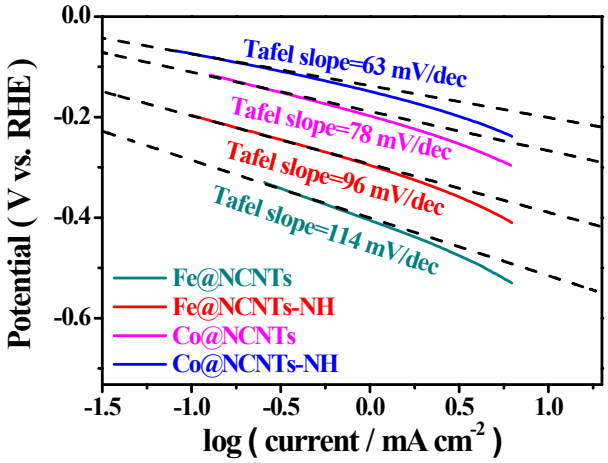

Figure S7. Tafel plots for Fe@NCNTs, Fe@NCNTs-NH, Co@NCNTs and Co@NCNTs-NH, respectively.

DFT calculation method

All calculations were performed using the Vienna Ab-initio Simulation Package (VASP).[8-11] The Perdew-Burke-Ernzerhof (PBE) functional[12, 13] for the exchange-correlation term was used with the projector augmented wave method[14, 15] and a cutoff energy of 400 eV. The model used in the calculation was shown in Figure S7a, which consists of CNT (6, 6) encapsulating a Fe_4 cluster. To investigate the effect of nitrogen doping, the CNT doped with the graphitic nitrogen was used as the calculated model. The supercells are in rectangular lattice, where a = b = 20 Å and c = 9.838 Å. A 1×1×24 Monkhorst-Pack k-point sampling was used for density of states (DOS) calculations and 1×1×4 for other calculations. All structures were fully relaxed to the ground state and spin-polarization was considered in all calculations. The convergence of energy and forces were set to 1×10^{-4} eV and 0.05 eV/Å, respectively. The effect of water was considered in illustrating the free energy profile of the reaction by adding a few water layers (Fig. S7b). The free energies of the intermediates were obtained by $\Delta G(H^*) = \Delta E(H^*)+\Delta ZPE-T\Delta S$, where $\Delta E(H^*)$, ΔZPE and ΔS is the binding energy, zero point energy change and entropy change of adsorption H, respectively. The ΔZPE and ΔS were obtained according to the method reported by Norskov et al. using normal-mode analysis with DFT calculation.[16] The vibrational entropy for H adsorbed on CNTs is less than 1 meV, so $\Delta S = S(H^*) - 1/2\ S(H_2) \approx - 1/2\ S(H_2)$. For H_2 at 300 K and 1 atm, $TS(H_2) = 0.41$ eV, then we get $T\Delta S \approx 0.20$ eV. We calculated the ZPE for H adsorbed on CNTs which is 0.31 eV, and for ZPE of H_2 we use the value 0.27 eV from Norskov, so ΔZPE for H* is $ZPE(H^*) - 1/2\ ZPE(H_2) = 0.17$ eV. This means that $\Delta G(H^*) = \Delta E(H^*) + 0.37$ eV. The transition state (TS) of each elementary reaction was searched using the dimer approach improved by Heyden et al. [17, 18] The center of the occupied band for projected DOS in Figure 3a is defined as the position where the occupied band (sum of C_{2p} and H_{1s}) is half-filled.

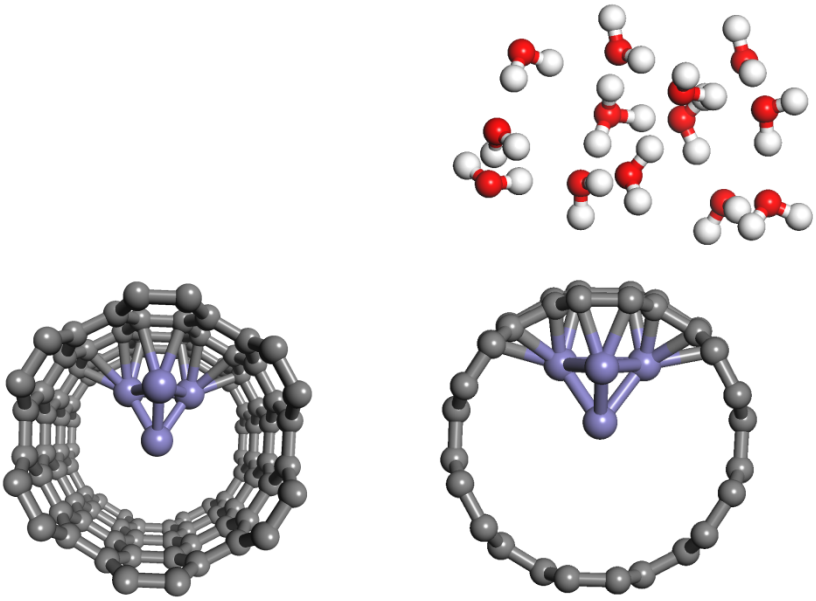

(a) (b)

Figure S8. (a) The calculation model of CNT (6, 6) encapsulating a Fe_4 cluster. (b) The calculation model with water layers. The gray balls represent C atoms, light blue for Fe, red for O and white for H.

Table S3. Adsorption free energy of H (ΔG(H*)) (in eV) for various models.

Structures	ΔG(H*)
Pure CNTs	1.29
NCNTs	0.42
Co@CNTs	0.18
Co@NCNTs	-0.15
FeCo@CNTs	0.11
FeCo@NCNTs	-0.02

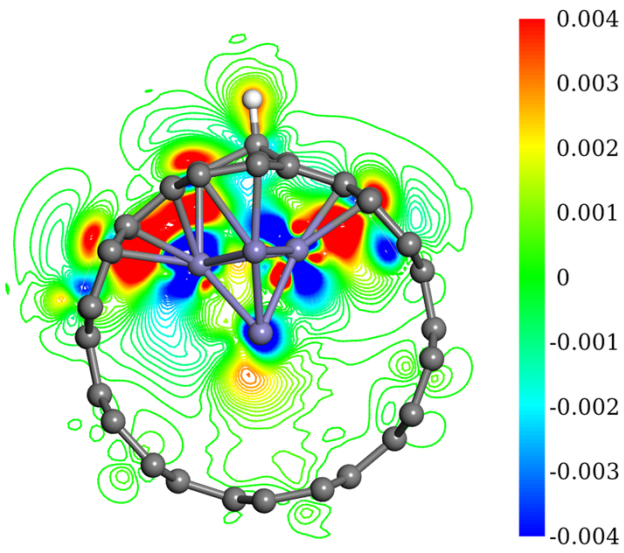

Figure S9. Difference in charge density (Δρ) of H adsorbed on Fe@CNTs with the blue and red areas denoting decreased and increased charge density, respectively. The Δρ is defined as Δρ = ρ(total) – ρ(H-CNTs) – ρ(Fe), where ρ(total), ρ(H-CNTs) and ρ(Fe) are charge densities of H-Fe@CNTs, H-CNTs and Fe cluster, respectively. This contour map shows that the electrons transfer from Fe cluster to CNTs and subsequently increase the charge density of the C-H bond.

Rererence

1. W. Chen, X. L. Pan, M. G. Willinger, D. S. Su and X. H. Bao, *J. Am. Chem. Soc.*, 2006, **128**, 3136-3137.
2. Y. G. Li, H. L. Wang, L. M. Xie, Y. Y. Liang, G. S. Hong and H. J. Dai, *J. Am. Chem. Soc.*, 2011, **133**, 7296-7299.
3. W. F. Chen, K. Sasaki, C. Ma, A. I. Frenkel, N. Marinkovic, J. T. Muckerman, Y. M. Zhu and R. R. Adzic, *Angew. Chem. Int. Ed.*, 2012, **51**, 6131-6135.
4. H. Vrubel and X. L. Hu, *Angew. Chem. Int. Ed.*, 2012, **51**, 12703-12706.
5. P. D. Tran, M. Nguyen, S. S. Pramana, A. Bhattacharjee, S. Y. Chiam, J. Fize, M. J. Field, V. Artero, L. H. Wong, J. Loo and J. Barber, *Energy Environ. Sci.*, 2012, **5**, 8912-8916.
6. K. K. Yong Zhao, Kazuhito Hashimoto, and Shuji Nakanishi, *Angew. Chem. Int. Ed.*, 2013, **52**, 13638-13641.
7. W. F. Chen, C. H. Wang, K. Sasaki, N. Marinkovic, W. Xu, J. T. Muckerman, Y. Zhu and R. R. Adzic, *Energy Environ. Sci.*, 2013, **6**, 943-951.
8. G. Kresse and J. Hafner, *Phys. Rev. B*, 1993, **47**, 558-561.
9. G. Kresse and J. Hafner, *Phys. Rev. B*, 1994, **49**, 14251-14269.
10. G. Kresse and J. Furthmuller, *Comp. Mater. Sci.*, 1996, **6**, 15-50.
11. G. Kresse and J. Furthmuller, *Phys. Rev. B*, 1996, **54**, 11169-11186.
12. J. P. Perdew, K. Burke and M. Ernzerhof, *Phys. Rev. Lett.*, 1996, **77**, 3865-3868.
13. J. P. Perdew, K. Burke and M. Ernzerhof, *Phys. Rev. Lett.*, 1997, **78**, 1396-1396.
14. P. E. Blochl, *Phys. Rev. B*, 1994, **50**, 17953-17979.
15. G. Kresse and D. Joubert, *Phys. Rev. B*, 1999, **59**, 1758-1775.
16. J. K. Norskov, T. Bligaard, A. Logadottir, J. R. Kitchin, J. G. Chen, S. Pandelov and J. K. Norskov, *J. Electrochem. Soc.*, 2005, **152**, J23-J26.
17. G. Henkelman and H. Jonsson, *J. Chem. Phys.*, 1999, **111**, 7010-7022.
18. A. Heyden, A. T. Bell and F. J. Keil, *J. Chem. Phys.*, 2005, **123**, 224101-224114.